15 Representative Elementary Watershed (REW) Approach: A New Blueprint for Distributed Hydrological Modelling at the Catchment Scale

HAKSU LEE, MURUGESU SIVAPALAN & ERWIN ZEHE

INTRODUCTION

The prediction of a catchment's response to atmospheric forcing, in the presence of a multiplicity of heterogeneous hydrological processes and nonlinear process interactions, remains a principal research focus in hydrology. In spite of considerable progress made in recent decades in understanding various processes and process interactions, our ability to make predictions in ungauged catchments remains limited. The reasons for this state of affairs are many and varied (Sivapalan *et al.*, 2003a). On the one hand, our ability to observe, explain and extrapolate hydrological processes is hampered by the lack of high quality data sets at sufficient resolution and in different hydrological regimes. On the other hand, observations in a limited number of experimental studies have shown that the dynamics of water flows in a watershed are extremely complex, nonlinear and highly variable in space and time, and cannot be satisfactorily described in terms of current hydrological theories developed at the laboratory scale, such as Darcy's law (Freer *et al.*, 2002; Kirchner, 2003). Therefore, further development of the field of catchment hydrology depends crucially on the development of advanced, rapid and cost-effective measurement techniques as well as rapid advances in hydrological theories that can deal with complex space–time variabilities and nonlinear process interactions. This chapter deals with the latter issue, and presents a new theoretical framework as a blueprint for the development of distributed, physically-based models that can effectively deal with the process heterogeneities and complexities exhibited by natural catchments.

The current generation of physically-based distributed models have, as their basis of model architecture, the model blueprint presented initially by Freeze & Harlan (1969). These distributed models have the distinct advantage that they explicitly consider conservation of both mass and momentum, albeit at the point or Representative Elementary Volume (REV) scale. In addition, they can also generate distributed predictions of state variables and water fluxes within the catchment, and due to this presumed physical basis, can potentially predict the effects of changes in climate and in landscape properties such as soil type, vegetation and land use, on the catchment's responses. Therefore, such distributed models are often regarded as most suitable for hydrological predictions. However, these traditional distributed, physically-based

models suffer from serious shortcomings. First, they tend to be highly over-parameterized, with infinite combinations of parameter values potentially yielding the same result, leading to a large parameter estimation problem (Beven, 1993). Secondly, distributed models require extensive amounts of input data relating to climatic and landscape properties, which may not be available in most catchments. On the other hand, in spite of the ability to generate distributed predictions of water fluxes and state variables, these predictions cannot be independently validated in the absence of distributed measurement of hydrological responses. There are also fundamental difficulties because of their dependence on laboratory or REV-scale theories of water movement, such as Darcy's law, based on uniform soils (Beven, 2002), when in fact soils in natural catchments are highly heterogeneous, exhibiting complex geologies and surface and bedrock topographies, dynamic macropore networks, etc. These often lead to highly nonlinear, and even threshold, behaviour, defying simple treatments based on uniformity and linearity. Finally, in many cases, predictions are only required at the catchment scale, and therefore the generation of distributed predictions represents an overkill for the claimed but dubious advantage of using physically-based models. A more detailed discussion of the advantages and limitations of physically-based distributed models can be found in Beven (1989) and Grayson *et al.* (1992).

Recently, Reggiani *et al.* (1998, 1999) have proposed a new unifying framework for watershed response studies and modelling through a systematic derivation of a new set of balance equations for mass, momentum, energy and entropy, including associated constitutive relationships for various exchange fluxes, at the scale of a well-defined spatial domain, which they called the Representative Elementary Watershed (REW). By deriving these equations from first principles (mass conservation, Newton's laws of motion, Second Law of Thermodynamics) with a minimum number of simplifying assumptions, the balance equations and constitutive relationships derived by Reggiani *et al.* are general enough to be applicable to a wide range of conditions. Secondly, by deriving the equations at the scale of the REW, namely the scale at which predictions are usually required and not at the point or REV scale, their theory has the potential to lead to models that are not overly complex in terms of the input data requirements, computational burden, and also in terms of the response measurements required for both external and distributed model validation. For these reasons, the theoretical framework presented by Reggiani *et al.* has been touted as having the potential to be the basis for a new generation of distributed, physically-based models operating directly at the catchment scale (Beven, 2002; Reggiani & Schellekens, 2003). Further investigation of Reggiani *et al.*'s theory, and its assessment as an acceptable physically-based model through application and validation in real catchments, is necessary to demonstrate its capabilities and its potential to overcome the problems of the current generation of distributed models. Therefore, the aim of this chapter is to present a review of the REW approach, followed by a survey of the various building blocks of a new model blueprint based on the REW approach, and a report on the progress that has been made recently towards its realization.

For hydrological models to be truly physically based their governing equations must be derived deductively from established physical principles, as defined by physical laws and physically meaningful assumptions, and in addition, they should produce results consistent with observations (Beven, 2002). The REW approach of Reggiani *et al.* satisfies the former but not yet the latter. Therefore it is important to

demonstrate that the REW approach, i.e. the balance equations and associated constitutive theory, will lead to numerical models that can generate predictions consistent with observations. This chapter documents the progress that has been made in this direction. In particular, it surveys the progress made towards: (1) the development of reasonable closure relations for the mass exchange fluxes within and between various REW sub-regions that effectively parameterize the effects of sub-REW heterogeneity of climatic and landscape properties; (2) numerical solution of the resulting governing equations, consisting of a set of coupled ordinary differential equations and algebraic equations for a number of REWs and the sub-regions within them; (3) approaches for the estimation of model parameters that are physically meaningful at the REW scale; (4) methodologies for the verification of the model predictions generated by the REW-scale model in an actual catchment; and (5) approaches to assess the reliability of the new model through estimation of model predictive uncertainty. Towards the end, this chapter also presents, for illustrative purposes, a preliminary application and validation of the new REW-scale model in an actual catchment in the southwest of Western Australia.

OVERVIEW OF THE REPRESENTATIVE ELEMENTARY WATERSHED APPROACH

We start with a brief review of the REW theory of Reggiani *et al.* (1998, 1999) based on their papers. Reggiani *et al.* (1998) define the Representative Elementary Watershed (REW) as the smallest and most elementary unit into which we can discretize the watershed for a given time scale of interest, and as the functional unit representative of other sub-entities of the entire watershed. The REW presented by Reggiani *et al.* (1998, 1999) is composed of five sub-regions, which are the unsaturated zone (u-zone), saturated zone (s-zone), concentrated overland flow zone (c-zone), saturated overland flow zone (o-zone) and channel zone (r-zone). These are defined on the basis of the various hydrological processes operating within the catchment, consisting of different physical characteristics and time scales. The ensemble of REWs constituting the catchment communicate with each other by exchanging mass, momentum and energy through the inlet and outlet sections of the associated channel reaches, and laterally through the exchange of groundwater and soil moisture across the soil mantle separating REWs. In addition, the sub-regions within each REW also exchange fluxes of mass, momentum and energy internally within the REW across the interfaces separating these sub-regions. Figure 15(a) presents the discretization of a catchment into three REWs (as an illustration) based on channel as well as catchment geometry, and Fig. 15(b) presents in more detail the assumed sub-regions making up the spatial domain of a typical REW, and the various mass exchange fluxes across sub-region and REW boundaries.

Following the division of the catchment into smaller entities, i.e. the REWs and associated sub-regions, the averaging approach is employed to derive the REW-scale balance equations for mass, momentum, energy and entropy. The distributed description into an ensemble of phases, sub-regions and REWs generates boundaries and requires jump conditions to characterize the transfer of mass, momentum, energy and entropy across these boundaries. These jump conditions are employed for the manipulation of the Second Law of Thermodynamics. Constitutive relationships are derived for the exchanges of mass, momentum and energy fluxes across these boundaries with

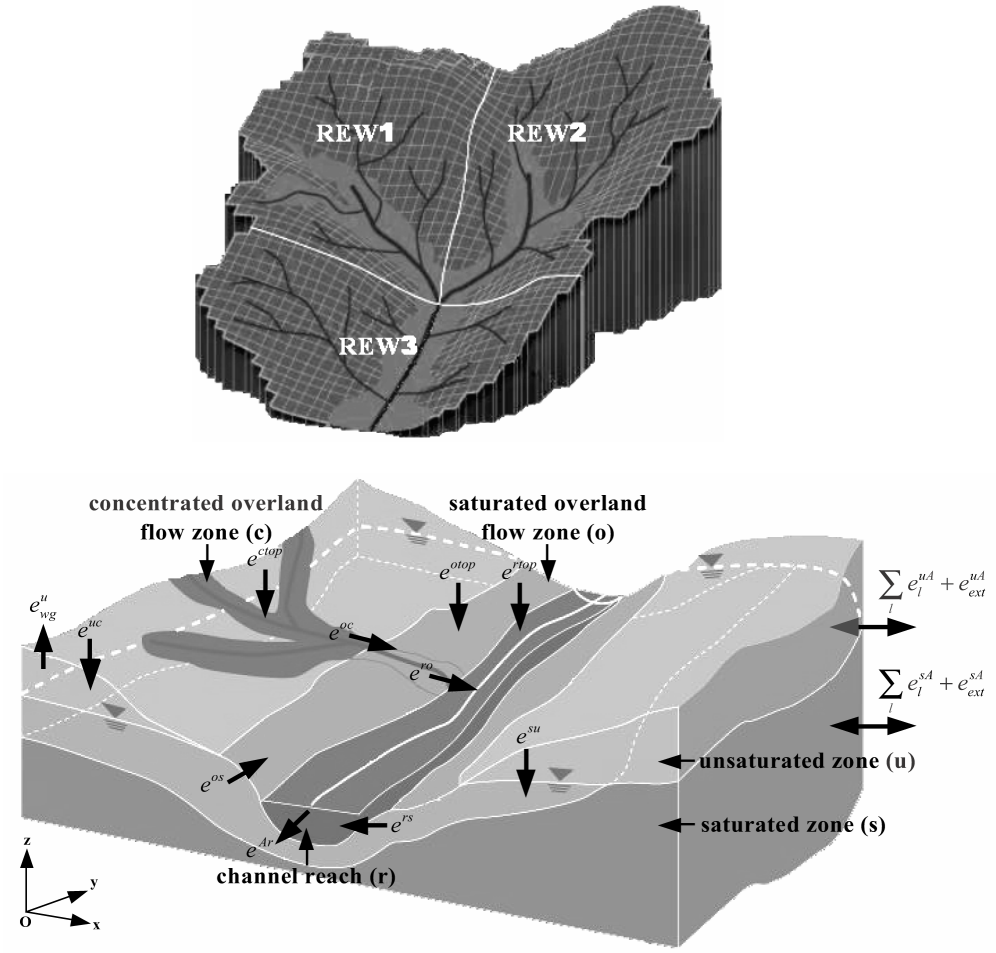

Fig. 15.1 *(a) Catchment discretization into three REW units. (b) Mass exchange fluxes and sub-regions making up the spatial domain of a REW (after Reggiani et al., 1999, 2000).* e^{uc} *denotes infiltration,* e^{u}_{wg} *evapotranspiration from unsaturated zone,* e^{su} *recharge or capillary rise,* e^{ctop}, e^{otop} *and* e^{rtop} *rainfall or evaporation at c, o and r-zones respectively,* e^{oc} *concentrated overland flow,* e^{ro} *saturated overland flow,* e^{os} *seepage flow,* e^{rs} *flow from saturated zone to channel,* e^{Ar} *channel flow at outlet, and* $\sum_l e^{uA}_l + e^{uA}_{ext}$ *and* $\sum_l e^{sA}_l + e^{sA}_{ext}$ *are mass exchanges across mantle segment at u and s-zones, respectively.*

the aid of the Second Law of Thermodynamics. Equilibrium expressions for the various momentum exchange terms are obtained by imposing conditions of thermodynamic equilibrium, and the non-equilibrium components of the momentum exchange fluxes are described as a first or second order function of velocity, depending on which type of flow is considered. In Reggiani *et al.* (1999), the closure relations governing the mass exchange terms are assumed to be linear functions of the differences in chemical and gravitational potentials and average velocities between the adjacent sub-regions (or REWs) based on entropy inequality. Finally, by substituting the parameterized mass

and momentum exchange terms into the respective conservation equations, and by projecting the momentum balance equations along the global reference system, the final set of parameterized balance equations for mass and momentum are obtained. Since the parameterized mass and momentum balance equations are composed of 13 equations and 23 unknowns, a set of 10 additional geometric relationships is introduced to produce a determinate system. The resulting set of 23 equations in 23 unknown REW-scale variables represent a system of coupled nonlinear ordinary differential and algebraic equations, and allow us to simulate the responses of the various sub-regions of the catchment and to generate space–time fields of storages and velocities everywhere across the catchment.

Simplified set of balance equations for mass and momentum balance

The resulting set of the REW-scale balances of mass and momentum and supplementary geometric relationships are summarized below; more details on the derivation procedure can be obtained from Reggiani *et al.* (1998, 1999). Definitions of the various coefficients and state variables are summarized in the nomenclature section at the end of this chapter and are omitted here for simplicity.

Saturated zone (s-zone) mass balance

$$\underbrace{\frac{\mathrm{d}}{\mathrm{d}t}(\rho\varepsilon y^s\omega^s)}_{\text{storage}} = \underbrace{A^{so}[p^o - p^s + \rho(\phi^o - \phi^s)]}_{\text{seepage}} - \underbrace{B^{us}\omega^u v_z^u}_{\substack{\text{exchag. with}\\ \text{unsat. zone}}} + \underbrace{A^{sr}[p^r - p^s + \rho(\phi^r - \phi^s)]}_{\text{sat. zone–river exchange}} + \underbrace{\sum_l B_l^{sA}\frac{1}{2}[\pm\mathbf{A}_{l,x}^{sA}(v_x^s + v_x^s|_l) + \pm\mathbf{A}_{l,y}^{sA}(v_y^s + v_y^s|_l)] + e_{ext}^{sA}}_{\text{exchange across mantle segments}} \tag{1}$$

Saturated zone (s-zone) momentum balance

$$\underbrace{\pm\sum_l \mathbf{A}_{l,\lambda}^{sA}[-p^s + \rho(\phi_l^{sA} - \phi^s)]}_{\text{inter–REW driving force}} + \underbrace{\pm\mathbf{A}_{ext,\lambda}^{sA}[-p^s + \rho(\phi_{ext}^{sA} - \phi^s)]}_{\text{force acting on the external boundary}} + \underbrace{\pm\mathbf{A}_{\lambda}^{s\,bot}[-p^s + \rho(\phi^{s\,bot} - \phi^s)]}_{\text{force at the bottom boundary}} = \underbrace{-R^s v_\lambda^s}_{\text{resistance to flow}} \quad ;\ \lambda = x, y \tag{2}$$

Unsaturated zone (u-zone) mass balance

$$\underbrace{\frac{\mathrm{d}}{\mathrm{d}t}(\rho y^u\omega^u s^u)}_{\text{storage}} = \underbrace{A^{uc}[p^c - p^u + \rho(\phi^c - \phi^u)]}_{\text{infiltration}} + \underbrace{B^{us}\omega^u v_z^u}_{\substack{\text{exchag. with}\\ \text{sat. zone}}} + \underbrace{A_{wg}^u(\mu_g^u - \mu_w^u)}_{\text{evaporation}} + \underbrace{\sum_l B_l^{uA}\frac{1}{2}[\pm\mathbf{A}_{l,x}^{uA}(v_x^u + v_x^u|_l) + \pm\mathbf{A}_{l,y}^{uA}(v_y^u + v_y^u|_l)] + e_{ext}^{uA}}_{\text{exchange across mantle segments}} \tag{3}$$

Unsaturated zone (u-zone) momentum balance

$$\underbrace{\pm\sum_l \mathbf{A}_{l,\lambda}^{uA}[-p^u + \rho(\phi_l^{uA} - \phi^u)]}_{\text{inter–REW driving force}} + \underbrace{\pm\mathbf{A}_{ext,\lambda}^{uA}[-p^u + \rho(\phi_{ext}^{uA} - \phi^u)]}_{\text{force acting on the external boundary}} = \underbrace{-R^u v_\lambda^u}_{\text{resistance to flow}} \quad ;\ \lambda = x, y \tag{4}$$

$$\underbrace{[-p^u-\rho(\phi^{uc}-\phi^u)]\varepsilon\omega^u}_{\text{force top}}-\underbrace{\rho\varepsilon s^u y^u\omega^u g}_{\text{gravity}}=\underbrace{-R^u v_z^u}_{\text{resistance force}} \tag{5}$$

Concentrated overland flow zone (c-zone) mass balance

$$\underbrace{\frac{\mathrm{d}}{\mathrm{d}t}(\rho y^c\omega^c)}_{\text{storage}}=\underbrace{-A^{uc}[p^c-p^u+\rho(\phi^c-\phi^u)]}_{\text{infiltration into unsat. zone}}-\underbrace{\frac{1}{4}B^{co}\Lambda^{co}(y^o+y^c)(v^o+v^c)}_{\text{flow to sat. overl. flow}}+\underbrace{\omega^c J}_{\text{rainfall or evaporation}} \tag{6}$$

Concentrated overland flow zone (c-zone) momentum balance

$$\underbrace{(\rho y^c\omega^c)\frac{\mathrm{d}v^c}{\mathrm{d}t}}_{\text{inertial term}}-\underbrace{\rho y^c\omega^c g\sin\gamma^c}_{\text{gravity}}=-\underbrace{U^c v^c\left|v^c\right|}_{\text{resistance to flow}} \tag{7}$$

Saturated overland flow zone (o-zone) mass balance

$$\underbrace{\frac{\mathrm{d}}{\mathrm{d}t}(\rho y^o\omega^o)}_{\text{storage}}=\underbrace{-B^{or}\Lambda^{or}y^o v^o}_{\text{lat. channel inflow}}+\underbrace{A^{so}[p^o-p^s+\rho(\phi^o-\phi^s)]}_{\text{seepage}}+\underbrace{\frac{1}{4}B^{co}\Lambda^{co}(y^o+y^c)(v^o+v^c)}_{\text{inflow from conc. overl. flow}}+\underbrace{\omega^o J}_{\text{rainfall or evaporation}} \tag{8}$$

Saturated overland flow zone (o –zone) momentum balance

$$\underbrace{(\rho y^o\omega^o)\frac{\mathrm{d}v^o}{\mathrm{d}t}}_{\text{inertial term}}-\underbrace{\rho y^o\omega^o g\sin\gamma^o}_{\text{gravity}}=-\underbrace{U^o v^o\left|v^o\right|}_{\text{resistance to flow}} \tag{9}$$

Channel reach (r-zone) mass balance

$$\underbrace{\frac{\mathrm{d}}{\mathrm{d}t}(\rho m^r\xi^r)}_{\text{storage}}=\underbrace{B^{or}\Lambda^{or}y^o v^o}_{\text{lateral inflow}}-\underbrace{A^{sr}[p^r-p^s+\rho(\phi^r-\phi^s)]}_{\text{channel–sat. zone exch.}}+\underbrace{\pm\sum_l B_l^{rA}\frac{1}{2}\mathbf{A}_l^{rA}(v^r+v^r|_l)+e_{ext}^{rA}}_{\text{inflow, outflow}}+\underbrace{\xi^r w^r J}_{\text{rainfall or evaporation}} \tag{10}$$

Channel reach momentum (r-zone) balance

$$\begin{aligned}\underbrace{(\rho m^r\xi^r)\frac{\mathrm{d}v^r}{\mathrm{d}t}}_{\text{inertial term}}&=\underbrace{\rho g m^r\xi^r\sin\gamma^r}_{\text{gravitional force}}-\underbrace{U^r v^r\left|v^r\right|}_{\text{Chezy resistance}}\\&+\underbrace{\pm\sum_l \mathbf{A}_l^{rA}\cos\delta_l[-p^r+\rho(\phi_l^{rA}-\phi^r)]}_{\text{pressure forces exchanged among REWs}}+\underbrace{\mathbf{A}_{ext}^{rA}[-p^r+\rho(\phi_{ext}^{rA}-\phi^r)]}_{\text{pressure force at watershed outlet}}\end{aligned} \tag{11}$$

Note in the above that equations (2) and (4) each represent a pair of equations for momentum balance in the x and y directions. The 13 REW-scale balance equations listed above include 23 unknowns, including eight velocity terms ($v_x^u, v_y^u, v_z^u, v_x^s, v_y^s, v^o$, v^c, v^r), the saturation degree in unsaturated zone (s^u), the volume of each zone divided by the horizontal projected area of REW ($y^u\omega^u$, $y^s\omega^s$, $y^c\omega^c$, $y^o\omega^o$, $m^r\xi^r$), the area fraction of each zone except for the channel reach (ω^u, ω^s, ω^c, ω^o), channel cross sectional area (m^r), channel width (w^r), channel depth (y^r), the length of the boundary separating the

two overland flow zones from each other (Λ^{co}), and the length of the curve forming the edge of the channel (Λ^{or}). This is an indeterminate system and requires an additional 10 relationships to make it mathematically tractable. The required number of additional relationships are obtained from geometrical considerations, and are summarized as follows (Reggiani *et al.*, 1999):

First geometric relationship Conservation of subsurface zone volume:

$$\frac{\mathrm{d}}{\mathrm{d}t}(y^u\omega^u)+\frac{\mathrm{d}}{\mathrm{d}t}(y^s\omega^s)=0 \tag{12}$$

Second geometric relationship Saturated surface area fraction as a function of saturated zone depth and its change rate:

$$\frac{\mathrm{d}\omega^o}{\mathrm{d}t}=f\left\{y^s,\frac{\mathrm{d}y^s}{\mathrm{d}t}\right\} \tag{13}$$

Third geometric relationship Complementarity of the areas of the two overland flow zones:

$$\Sigma^o+\Sigma^c=\Sigma \tag{14}$$

Fourth geometric relationship Conservation of the overland flow zone area:

$$\frac{\mathrm{d}\omega^o}{\mathrm{d}t}+\frac{\mathrm{d}\omega^c}{\mathrm{d}t}=0 \tag{15}$$

Fifth geometric relationship Concentrated overland flow zone is overlapping with the unsaturated zone area:

$$\omega^u=\omega^c \tag{16}$$

Sixth geometric relationship Drainage density as a function of average channel cross sectional area and its change rate:

$$\frac{\mathrm{d}\xi^r}{\mathrm{d}t}=f\left\{m^r,\frac{\mathrm{d}m^r}{\mathrm{d}t}\right\}, \text{ for first order channels and } \xi^r = \text{a constant, for higher order channels} \tag{17}$$

Seventh geometric relationship Average channel depth as a function of discharge:

$$y^r=a(m^rv^r)^b \tag{18}$$

Eighth geometric relationship Average channel width as a function of discharge:

$$w^r=\bar{c}(m^rv^r)^{\bar{d}} \tag{19}$$

Note that the coefficients $a,\bar{c}$ and exponents $b,\bar{d}$ in equations (18) and (19) must be evaluated from field data.

Ninth geometric relationship Boundary separating the two overland flow zones as a function of the fraction of area producing saturated overland flow:

$$\Lambda^{co}=f\left\{\omega^o\right\} \tag{20}$$

Tenth geometric relationship Boundary curve forming the edge of the channel as a function of average channel width and drainage density:

$$\Lambda^{or} = f\left\{w^r, \xi^r\right\} \tag{21}$$

Also, the saturated zone was assumed to underlie the whole of the REW; this leads to:

$$\omega^s = 1 \tag{22}$$

It should be noted that the REW-scale mass balance equations (1), (3), (6), (8) and (10) are a parameterized form of mass balance equations for the s-, u-, c-, o- and r-zones, respectively, and were obtained by expressing the various exchange fluxes amongst the different REW sub-regions, denoted as e^{ij}, in terms of the differences in chemical and gravitational potentials and average velocities between the adjacent sub-regions. Since in this chapter we plan to relax the linearization assumption of these exchange fluxes, we revert back to a more general set of mass balance equations presented by Reggiani *et al.* (1998); we thus replace equations (1), (3), (6), (8) and (10) by equations (23), (24), (25), (26) and (27) presented below:

$$\underbrace{\frac{\mathrm{d}}{\mathrm{d}t}(\rho\varepsilon y^s \omega^s)}_{\text{storage}} = \underbrace{e^{so}}_{\text{seepage}} + \underbrace{e^{su}}_{\substack{\text{exchag. with}\\ \text{unsat. zone}}} + \underbrace{e^{sr}}_{\text{sat. zone}-\text{river exchange}} + \underbrace{\sum_l e_l^{sA} + e_{ext}^{sA}}_{\text{exchange across mantle segments}} \tag{23}$$

$$\underbrace{\frac{\mathrm{d}}{\mathrm{d}t}(\rho\varepsilon y^u \omega^u s^u)}_{\text{storage}} = \underbrace{e^{uc}}_{\text{infilteration}} + \underbrace{e^{us}}_{\substack{\text{exchag. with}\\ \text{sat. zone}}} + \underbrace{e_{wg}^{u}}_{\text{evaporation}} + \underbrace{\sum_l e_l^{uA} + e_{ext}^{uA}}_{\text{exchange across mantle segments}} \tag{24}$$

$$\underbrace{\frac{\mathrm{d}}{\mathrm{d}t}(\rho y^c \omega^c)}_{\text{storage}} = \underbrace{e^{cu}}_{\text{infilteration into unsat. zone}} + \underbrace{e^{co}}_{\text{flow to sat. overl. flow}} + \underbrace{e^{ctop}}_{\text{rainfall or evaporation}} \tag{25}$$

$$\underbrace{\frac{\mathrm{d}}{\mathrm{d}t}(\rho y^o \omega^o)}_{\text{storage}} = \underbrace{e^{or}}_{\text{lat. channel inflow}} + \underbrace{e^{os}}_{\text{seepage}} + \underbrace{e^{oc}}_{\text{inflow from conc. overl. flow}} + \underbrace{e^{otop}}_{\text{rainfall or evaporation}} \tag{26}$$

$$\underbrace{\frac{\mathrm{d}}{\mathrm{d}t}(\rho m^r \xi^r)}_{\text{storage}} = \underbrace{e^{ro}}_{\text{lateral inflow}} + \underbrace{e^{rs}}_{\text{channel}-\text{sat. zone exch.}} + \underbrace{\sum_l e_l^{rA} + e_{ext}^{rA}}_{\text{inflow, outflow}} + \underbrace{e^{rtop}}_{\text{rainfall or evaporation}} \tag{27}$$

BUILDING BLOCKS OF THE REW APPROACH AS A NEW MODEL BLUEPRINT

In this section, we present the building blocks required to transform the REW-scale balance equations presented above into a blueprint for the development of a new distributed physically-based model at the catchment scale. Section 1 discusses methodologies for the development of appropriate, physically-reasonable closure relations for various mass exchange fluxes, incorporating the effects of the spatial heterogeneity of climate and landscape properties through the process of upscaling. Section 2 summarizes the revised balance equations with the inclusion of the newly developed closure relations taken from a companion paper (Lee *et al*., 2005a), and Section 3 discusses the development of a numerical model that solves the resulting coupled set of ordinary differential equations, while Sections 4 and 5 deal,

respectively, with the issue of parameter estimation and the application (calibration and validation) of the REW-scale model in actual catchments. The final section (6) discusses the assessment of model reliability through measures of model predictive uncertainty.

1. Development of closure relations for mass exchange fluxes

Achieving appropriate closure relations for the mass exchange fluxes is a critical component of the REW approach. Examples of fluxes for which closure relations are required include infiltration, bare soil evaporation, transpiration, groundwater recharge or capillary rise, infiltration excess overland flow, saturation excess overland flow, seepage outflow (subsurface storm flow), channel flow, and groundwater discharge. In developing these closure relations, we seek to define functional relationships between the given mass exchange fluxes and relevant state variables (soil moisture, velocity) for the sub-regions of interest. The effects of spatial heterogeneities of landscape properties (soil, topography, vegetation) at scales smaller than the REW need to be incorporated into their parameterizations. Similarly, rapid fluctuations of the system response at time scales smaller than the averaging interval used in the framework also need to be parameterized (Reggiani *et al.*, 1998).

Reggiani *et al.* (1999, 2000) presented closure relations developed on intuitive grounds and expressed as linear functions of the mean values of the velocities on both sides of the boundary, and of the difference in hydraulic potentials. However, there was no effort made to connect these to ground reality, and especially to capture the effects of sub-REW and sub-time variability. Besides, the assumption of linear dependence is highly restrictive in the light of field evidence that shows strong nonlinearities, including threshold behaviour, in observed catchment behaviour. Therefore, considerable new work needs to be conducted on upscaling approaches towards the development of physically reasonable closure relations that connect process descriptions at the REW-scale to the heterogeneity of climatic and landscape properties .

The upscaling methods currently available for developing closure relations can be classified into four categories: field experiments, theoretical/analytical derivations, numerical experiments, and hybrid approaches. The field experimental approach seeks to find closure relations from the analysis of data obtained in the field, either in a routine manner or through focused intensive field experiments (Duffy, 1996). Empirical closure relations based on field observations may be the best candidates for the REW-scale closure relations, because they best represent the intrinsic natural variability occurring within actual catchments.

In the theoretical/analytical approach, the emphasis is on deriving closure relations through analytical integration or upscaling of small-scale physically-based equations. It has the advantage that the resulting closure relations, as well as the consequent REW-scale parameters, retain some or most of their traditional meaning, and therefore there is a chance that they can be estimated by referring back to a possible mapping between landscape and/or climatic properties and model parameters. On the other hand, the numerical simulation approach seeks to derive closure relations based on simulated data sets that could be generated through application of distributed physically-based hydrological models, based on small-scale physical theories, under well defined boundary conditions (Duffy, 1996; Kees *et al.*, 2002, 2004; Zehe *et al.*, 2005). Finally, the hybrid approach represents a combination of any of the above approaches.

2. *Balances of mass and momentum at the REW scale with revised closure relations*

We used a variety of methods to develop closure relations for infiltration, exfiltration (bare soil evaporation and transpiration), groundwater recharge or capillary rise, infiltration excess overland flow, saturation excess overland flow, seepage outflow (subsurface storm flow), and channel flow. The detailed derivation procedures used for the new closure relations can be found in a separate chapter (Lee *et al.*, 2005a). For the sake of brevity, neither the derivation procedure nor the resulting closure relations for the various mass exchange fluxes is presented in this paper. Instead, the final forms of the mass and momentum balance equations, after including the new closure relationships, are presented in equations (28) to (36) below:

Saturated zone mass balance equation

$$\underbrace{\frac{\mathrm{d}}{\mathrm{d}t}(\varepsilon y^s \omega^s)}_{\text{storage}} = \underbrace{-\alpha^{us}\varepsilon\omega^u v_z^u}_{\text{recharge or capillary rise}} \underbrace{-\omega^o \alpha_1^{os} \overline{K_s}^{\alpha_2^{os}} \left[\frac{y^u s^u \omega^u + y^s}{Z\Psi}\right]^{\alpha_3^{os}}}_{\text{seepage}} - \underbrace{q_s}_{\text{sat. zone}-\text{river exchange}} \tag{28}$$

Unsaturated zone mass balance equation

$$\underbrace{\frac{\mathrm{d}}{\mathrm{d}t}(y^u \varepsilon \omega^u s^u)}_{\text{storage}} = \underbrace{min\left[i\omega^u,\ \omega^u \overline{K_s}\left(1+\alpha^{uc}\frac{\Psi(1-s^u)\varepsilon}{s^u y^u}\right)\right]}_{\text{infiltration}} + \underbrace{\alpha^{us}\varepsilon\omega^u v_z^u}_{\text{recharge or capillary rise}} \underbrace{-min\left[\omega^u\left(e_p + Mk_v\overline{e_p}\right),\ \alpha_{wg}^u \frac{\omega^u \overline{K}_s}{(1-s^u)y^u}\frac{(s^u)^{2+d}\varepsilon\Psi_b}{m}\right]}_{\text{evapotranspiration}} \tag{29}$$

Unsaturated zone momentum balance equation

$$v_z^u = \overline{K}\frac{s^u}{y^u}\{\Psi - \frac{1}{2}y^u\} \tag{30}$$

Concentrated overland flow zone mass balance equation

$$\underbrace{\frac{\mathrm{d}}{\mathrm{d}t}(y^c\omega^c)}_{\text{storage}} = \underbrace{\omega^c J}_{\text{rainfall or evaporation}} \underbrace{-min\left[i\omega^u,\ \omega^u\overline{K_s}\left(1+\alpha^{uc}\frac{\Psi(1-s^u)\varepsilon}{s^u y^u}\right)\right]}_{\text{infiltration}} - \underbrace{\alpha^{oc}\xi^r y^c v^c}_{\text{flow to saturated overland flow zone}} \tag{31}$$

Concentrated overland flow zone momentum balance equation

$$v^c = \frac{1}{n^c} y^{c\,2/3} sin(\gamma^c)^{1/2} \tag{32}$$

Saturated overland flow zone mass balance equation

$$\underbrace{\frac{\mathrm{d}}{\mathrm{d}t}(y^o\omega^o)}_{\text{storage}} = \underbrace{\omega^o\alpha_1^{os}\overline{K_s}^{\alpha_2^{os}}\left[\frac{y^u s^u\omega^u + y^s}{Z\Psi}\right]^{\alpha_3^{os}}}_{\text{seepage}} + \underbrace{\alpha^{oc}\xi^r y^c v^c}_{\text{inflow from conc. overl. flow}} + \underbrace{\omega^o J}_{\text{rainfall or evaporation}} - \underbrace{\alpha^{ro}\xi^r y^o v^o}_{\text{lateral channel inflow}} \tag{33}$$

Saturated overland flow zone momentum balance equation

$$v^o = \frac{1}{n^o} y^{o\,2/3} sin(\gamma^o)^{1/2} \tag{34}$$

Channel zone mass balance equation

$$\underbrace{\frac{\mathrm{d}}{\mathrm{d}t}(m^r\xi^r)}_{\text{storage}} = \underbrace{\alpha^{ro}\xi^r y^o v^o}_{\text{lateral channel inflow}} + \underbrace{q_s}_{\text{sat. zone–river exchange}} + \underbrace{\sum_l \frac{m_l^r v_l^r}{\Sigma}}_{\text{inflow}} - \underbrace{\frac{m^r v^r}{\Sigma}}_{\text{outflow}} + \underbrace{\xi^r w^r J}_{\text{rainfall, evaporation on free surface}} \tag{35}$$

Channel zone momentum balance equation

$$v^r = \frac{1}{n^r}\sqrt{\frac{\left[\overline{R^r}\right]^{1/3}}{P^r l^r}}\left[m^r l^r \sin(\gamma^r) \pm \sum_l \{\frac{1}{4} y^r (m^r + m^l)\cos\delta_l\} - \frac{1}{2} y^r m^r \right] \tag{36}$$

In doing so, note that the 13 mass and momentum balance equations, (1) to (11), have been reduced to just nine by excluding the momentum balance equations in the horizontal direction in the two subsurface zones. The momentum balance equation (5) has been rewritten as equation (30) by following the procedure adopted by Reggiani *et al.* (2000). The momentum balance equations for the c-, o- and r-zones, i.e. equations (7), (9) and (11), respectively, have been simplified as equations (32), (34) and (36), by ignoring the inertial term, thus adopting the kinematic wave approximation, and by adopting the relationship between the Darcy-Weisbach friction factor and Manning coefficient for the second-order friction term, U^i, $i = c,o,r$ as $\xi_f^i = 8g(n_m^i)^2(\overline{R^i})^{-1/3}$, $i = c,o,r$. The procedure to convert the momentum balance equation for the channel reach, equation (11), into equation (36), is presented in Reggiani *et al*. (2001). Thus, equations (32) and (34) are the REW-scale Manning's equation for the movement over c- and o- zones, respectively, while equation (36) is the REW-scale diffusive wave equation for channel flow.

3. Numerical implementation based on balance equations

The REW-scale mass balance equations (28), (29), (31), (33) and (35), and the simplified momentum balance equations (30), (32), (34) and (36), constitute a coupled set of ordinary differential equations, combined with a set of algebraic equations for geometric relationships, equations (12) to (21). A critical problem is that the solution of the above set of governing equations has to deal with slow flow processes such as groundwater flow and unsaturated zone dynamics, and fast flow processes such as channel flow and overland flow. Such a wide range of time scales associated with the processes can make the system of coupled differential equations "stiff", due to the large differences in their eigen values associated with the system of equations. Stiff differential systems require us to adopt highly stable numerical schemes, since stability becomes more critical than accuracy. Many numerical methods, e.g. variable step variable order (VSVO) methods for second order systems (Thomas & Gladwell, 1985), exponential time differencing (Cox & Matthews, 2002) and the Rosenbrock method (1963), have been developed for solving stiff systems of differential equations. At the same time, computation time will also be very high if we use complicated numerical schemes for the coupled equations.

In our work we decided to trial simple numerical schemes at first, and by checking the error size and stability of the solution, more precise and stable numerical schemes could be progressively introduced. In this way, the numerical methods adopted can be

evaluated progressively, and the most optimal scheme that minimizes error size and computation time, while maintaining stability at all times, could be chosen to solve the set of coupled equations. The current version of the model uses a fourth-order Runge-Kutta method. Details on the numerical implementation of the REW equation system adopted so far are presented in a companion paper (Lee *et al*., 2005b).

4. Methods for parameter estimation

The governing equations in the REW approach includes many parameters, and their number will doubtless increase when we incorporate the effects of sub-grid scale variability and try to reproduce observed nonlinearities in the system response. As the number of parameters increases, their estimation becomes more difficult due to process interactions and interdependency of parameters. However, unlike other catchment-scale models such as HBV (Bergström, 1995), UP (Ewen, 1997) and LASCAM (Sivapalan *et al.*, 1996), the distributed model based on the REW approach will have the distinct advantage that, at least in principle, its parameters are physically meaningful and are measurable at the catchment-scale. Methods to estimate the various parameters of the REW-scale model will involve a combination of two alternative approaches: downward and upward.

The downward approach attempts to estimate the parameters through systematic analysis of observed streamflow data. The exact estimation procedure may vary, from manual calibration or application of inverse techniques on parts of the data, to automatic calibration on complete data series using sophisticated schemes such as NLFIT (Kuczera & Parent, 1998) and SCA (Duan *et al.*, 1992). Partial analysis of the observed streamflow record involves the analysis of signatures of variability, such as recession curves, plots of inter-annual variability, mean monthly variations (i.e. regime curve), flow duration curve, etc. These signatures provide a window into different aspects of catchment behaviour, and can help estimate smaller, non-overlapping subsets of the entire parameter set, without interference by other processes or parameters. The suggested analysis mirrors, when carried out in a hierarchical manner, the downward approach to hydrological modelling outlined in a number of previous papers (Jothityangkoon *et al.*, 2001; Atkinson *et al.*, 2002; Farmer *et al.*, 2003; Sivapalan *et al.*, 2003b). In another related example, Troch *et al.* (1993) found catchment scale hydraulic conductivity values and the initial storage capacity of a basin by matching a model based on the Boussinesq equation with observed streamflow recession curves.

On the other hand, the fact that the parameters of the REW-scale model are physically meaningful, representing basic physical laws in real catchments, offers some hope that the parameters can be estimated by recourse to analysis of actual landscape properties, i.e. soils, topography, vegetation, etc., which are measurable in the field. We will call this the upward approach. Underlying this approach is the assumption that the model parameters account for the effects of sub-grid variations of landscape properties, and are indeed sensitive to changes in the fine-scale property data (Ewen *et al.*, 1999). Further investigation is needed to connect measurable landscape properties and model parameters, including any parameter values inferred by inverse analysis (i.e. calibration). This investigation can be assisted by the use of detailed, physically-based simulation models, of the kind already used in the derivation of the closure relations (e.g. Duffy, 1996; Lee *et al.*, 2005a; Zehe *et al.*, 2005).

5. Application of model to real catchments

It is important for the credibility of the REW model framework that the resulting model be shown to produce realistic reproductions of observed catchment response, in a variety of catchments in different climatic/hydrological settings. There are two approaches to conduct the verification of the model predictions. The usual method is to use a selected portion of the data for model estimation (i.e. calibration), and then verify the performance on another part of the data record (i.e. validation). This is usually referred to as a split-sample test (Sorooshian & Gupta, 1995). The purpose of a split-sample test is to investigate model convergence to the data recorded.

An alternative approach to verification of the model performance is to compare the aggregated model results (i.e. REW-scale model), with those of a detailed, distributed physically-based distributed model operating at the point or REV scale. This can be done by integrating or averaging, up to the REW-scale as the case may be, the state variables and mass exchange fluxes generated by a detailed model, then comparing them against predictions by the REW model. For example, Ichikawa & Shiiba (2002) found good agreement between the predictions of a large-scale model that was obtained by lumping a kinematic wave equation model, and the aggregated values obtained from a fully distributed model. Kees *et al.* (2004) developed hillslope-scale balance equations and showed how the dynamics of subsurface storage obtained from this model compared well against those generated from a detailed physically-based distributed model.

An approach that is often neglected is to compare the spatially distributed predictions of the model against spatially distributed observations, where they exist. This not only involves comparing event or continuous streamflow hydrographs and temporal signatures thereof, but also spatial patterns, such as scaling behaviour of flood peaks with catchment area, hydrograph attenuation characteristics, dynamics of saturation areas, etc. These test different aspects of model performance, and can further improve the physical realism of the model. These are in addition to model reproduction of various temporal signatures, e.g. inter-annual variability, mean monthly variation, flow duration curve, etc., which are very useful indicators of catchment response, and can yield insights that may be missed by traditional split-sample tests.

6. Assessment of model reliability and predictive uncertainty

Hydrological models often need to be applied to storms and catchments outside of the range of conditions under which they have been successfully tested, such as for flood forecasting, design flood estimation and the generation of synthetic flows for water resources assessment. When using a model for extrapolation, it is essential to assess the reliability of the model output due to various sources of uncertainty. Generally there are three types of uncertainties affecting model reliability. These are input data uncertainty, model parameter uncertainty and model structure uncertainty. For assessing model output reliability the joint probability distributions (of climate inputs, model parameters and model structure) should be obtained for all the significant sources of uncertainty. However, the determination of these probability distribution functions is normally very difficult to almost impossible. Therefore, the estimation of predictive uncertainty as a measure of overall model reliability must be done in an approximate manner. Methods available for this are Monte Carlo simulation, Latin

hypercube sampling, mean-value first-order second-moment method, advanced first-order second-moment method, regional sensitivity analysis, and Rosenblueth's and Harr's point estimation method, etc. In particular, tools such as NLFIT (Kuczera & Parent, 1998), GLUE (Beven & Binley, 1992) and BaRE (Thiemann *et al.*, 2001) are now widely used to estimate model predictive uncertainty, and to assess the contributions of parameter uncertainty, input uncertainty, and model structure uncertainty. These will be carefully evaluated and adopted as part of the development of the REW model blueprint.

In addition to the overall uncertainty assessment, it is also important to identify key uncertainty sources because high levels of uncertainty in the input data and model parameters may cause poor model verification results. For achieving this purpose, the methods mentioned above could be used for inferring key uncertainty sources. For example, Beven & Binley (1992) applied regional sensitivity analysis to the Institute of Hydrology Distributed Model (IHDM) to determine key parameters by calibration and to perform uncertainty estimation. It is also important to check whether the uncertainty bounds of model predictions include the physically observable range of state variables by comparing observed values with simulated results. Comparison of simulated state variables, such as water table depth, with the observed values, will indicate whether the model is consistent with reality, i.e. whether the model is truly physically based.

PRELIMINARY TESTS OF CLOSURE RELATIONS AND MODEL PERFORMANCE

Tests of the adopted closure relations for physical reasonableness

The REW-scale balance equations for mass and momentum, equations (28) to (36), and geometric relations, equations (12) to (21), were solved by the fourth-order Runge-Kutta integration method, with 5 minutes as the calculation time step. A series of numerical experiments were carried out with the complete numerical model, with the view to exploring the physical reasonableness of the derived closure relations, and to see how they respond to different combinations of climate, soil, vegetation and topography. We present the results for two of these closure relations here: one for infiltration and runoff generation, and the second for seepage flux and the saturated area fraction. These were carried out at the event scale for hypothetical rainfall events, and for a hypothetical catchment. The parameter values used in this sensitivity study are presented in Table 15.1. For more details the reader is referred to Lee *et al.* (2005a).

1. Infiltration and surface runoff generation

Sensitivity analyses with respect to the closure relationship for infiltration were designed to explore the response of the infiltration component within the REW modelling framework to changes in the antecedent soil moisture content (AMC), rainfall intensity, and soil type. For these analyses, the following fixed parameter values were used: $DI = 2$, $t_r = 2$ days, $t_b = 8$ days, vegetation fraction $M = 1$, $z^r = 21$ m, $\beta_1^{\omega^o} = 0.3$, $\beta_2^{\omega^o} = 0.3$, $\beta_3^{\omega^o} = 0.4$, $\alpha^{uc} = 0.1$, $\alpha_{wg}^{u} = 5$, $\alpha_1^{os} = 10$ and $\alpha_2^{os} = 6.2$, where DI is the climatic dryness index, defined as the ratio of total annual potential evaporation to total annual precipitation. The remaining parameters and input information are summarized in Table 15.1.

Table 15.1 *Values of parameters, input data and initial conditions used in the sensitivity analyses.*

Group	Description		Value	Ref.
Soil	K_S saturated hydraulic conductivity (m s^{-1})	Silty loam	3.4 x 10^{-6}	Bras (1990)
		Sandy loam	3.4 x 10^{-5}	
		Sand	8.6 x 10^{-5}	
	Ψ_b bubbling pressure head (m)	Silty loam	0.45	
		Sandy loam	0.25	
		Sand	0.15	
	ε porosity (m^3 m^{-3})	Silty loam	0.35	
		Sandy loam	0.25	
		Sand	0.20	
	m pore size distribution index	Silty loam	1.2	
		Sandy loam	3.3	
		Sand	5.4	
	c pore disconnectedness index	Silty loam	4.7	
		Sandy loam	3.6	
		Sand	3.4	
	$s^u(0)$ initial soil moisture content in u-zone		0.0/0.05/0.1/0.15/0.2/0.5	
Climate	i precipitation intensity (mm h^{-1})		10/15/20/25/30	
	DI climatic dryness index		0.5/2.0	
	t_r storm period (day)		1/2	
	t_b inter-storm period (day)		4/8	
	t_a (= t_r + t_b) climatic period (day)		5/10	
Vegetation	M canopy density		0/1	
	k_v ratio of potential rates of transpiration and soil surface evaporation		1	
Hydraulic	n^c Manning roughness coefficient in c-zone ($m^{-1/3}$ s)		0.07	Chow *et al*. (1988)
	n^o Manning roughness coefficient in o-zone ($m^{-1/3}$ s)		0.035	
	n^r Manning roughness coefficient in r-zone ($m^{-1/3}$ s)		0.03	
	q_s steady flow from saturated zone to channel reach (mm h^{-1})		0.00012	
Geographic	Z average thickness of subsurface zone (m)		8	
	z^r average elevation of channel bed from datum (m)		21/25	
	z^s average elevation of the bottom end of REW from datum (m)		20	
	$y^s(0)$ initial average thickness of saturated zone (m)		$z^r - z^s$	
	$\beta_1^{\omega^o}$ parameter in geometric relation for saturated surface area		0.3/0.59942	
	$\beta_2^{\omega^o}$ parameter in geometric relation for saturated surface area		0.3/0.81443	
	$\beta_3^{\omega^o}$ parameter in geometric relation for saturated surface area		0.4/1.92196	
Flux closure	α^{uc} parameter in closure relation for e^{uc}		0.1/1.0/5.0	
	α_{wg}^u parameter in closure relation for e_{wg}^u		5/100	

Table 15.1 *(continued).*

α^{us} parameter in closure relation for e^{us}	1
α^{oc} parameter in closure relation for e^{oc}	1.5
α^{ro} parameter in closure relation for e^{ro}	2.5
α_1^{os} parameter in closure relation for e^{os}	10/2000
α_2^{os} parameter in closure relation for e^{os}	5.2/6.2
α_3^{os} parameter in closure relation for e^{os}	2.7

Figure 15.2(a) shows the effect of antecedent moisture content (AMC) of the unsaturated zone on the rate of infiltration, for silty loam, for an event with constant rainfall intensity of 15 mm h^{-1}. The results show that the infiltration rate decreases with

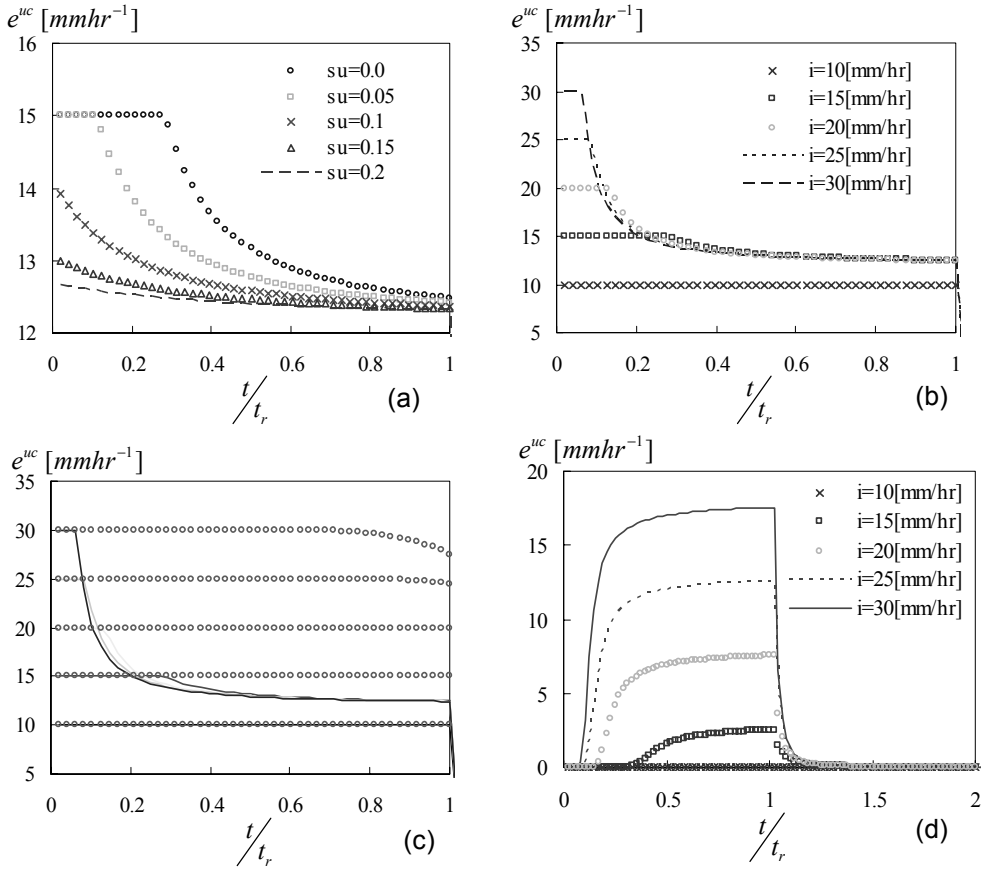

Fig. 15.2 *Sensitivity analysis on closure relation for infiltration and concentrated overland flow: (a) the effect of antecedent moisture content on the closure relation for infiltration process: silty loam; (b) climate effect on the closure relation for infiltration process: silty loam; (c) the effect of different soil on the closure relation for infiltration process: solid line for silty loam, circle for sand; (d) climate effect on the closure relation for concentrated overland flow: silty loam.*

increase of the AMC, and that the infiltration rate decreases exponentially to an asymptotic value after the surface is ponded. Figure 15.2(b) shows the effect of rainfall intensity on infiltration rate for silty loam when the AMC is zero. The results show that the time to surface ponding is shortened as the rainfall intensity increases, and that the infiltration rate approaches the same asymptotic value at large time, except for very low precipitation intensities, i.e. 10 mm h^{-1}, in which case all precipitation is infiltrated.

Figure 15.2(a) and (b) represent expected, indeed well known, infiltration behaviour. Figure 15.2(c) shows the effect of two different soil types, silty loam (solid line) and sand (circle), under different rainfall intensities, and zero AMC. It shows that the infiltration rate is higher for sandy soils because of higher infiltration capacity. Figure 15.2(d) shows Hortonian overland flow corresponding to Fig. 15.2(b). Hortonian overland flows closely mirror the infiltration behaviour over the concentrated overland flow zone. On the whole, the water dynamics within the concentrated overland flow zone is qualitatively well captured by the adopted closure relations for infiltration capacity and concentrated overland flow. These results confirm that the adopted closure relations do reproduce expected behaviour, and give us confidence that with the correct choice of parameter values the model can reproduce observed behaviour in actual catchments.

2. *Seepage flux and saturated area fraction*

Figures 15.3 and 15.4 are the results of sensitivity analyses with respect to the closure relations for saturated area fraction and seepage flux. For these analyses, climatic inputs and fixed parameter values were set as follows: antecedent moisture content, AMC = 0.5, i = 20 mm h^{-1}, t_r = 1 day, t_b = 4 days, climatic dryness index DI = 2.0, vegetation cover M = 1, α^{uc} = 1, α^{u}_{wg} = 100, α^{os}_{1} = 2000 and α^{os}_{2} = 5.2. The remaining parameter values are presented in Table 15.1. Firstly, since the seepage outflow is dependent upon the growth of the area of the seepage face as the water table rises, two functional forms for saturated area were tested, to see the effects of different topographies. One is a linear function; the resulting relationship is shown in Fig. 15.3(a). The use of nonlinear function relating topography to saturated area led to the results presented in Fig. 15.3(b). We see that initially the saturated area is larger for the linear case than for the nonlinear case and the difference becomes even larger as the water table rises. The results in Fig. 15.3 suggest that the linear functional form for topography may over-estimate the actual exchange fluxes through the seepage face.

Sensitivity analyses were then carried out with the REW-scale model to explore the effects of different soil types and topographies on seepage flux and saturation areas. Figures 15.4(a) to (c) present the response of seepage flux for two different topographies, linear and nonlinear, and three different soils, silty loam, sandy loam and sand. The corresponding variations of saturated area are presented in Fig. 15.4(d). They show that seepage flux is quicker and larger in volume under linear topography; this is because the fraction of saturated area is larger under linear topography than under nonlinear topography for the same average thickness of the saturated zone. For the case of sand, shown in Fig. 15.4(c), the seepage flux shows shorter time to peak and a higher peak flow than the other soil types, caused mainly by higher hydraulic conductivity and smaller suction pressure head. In this case, the difference between the linear and nonlinear topographies is much less than the others. The delay in the peak

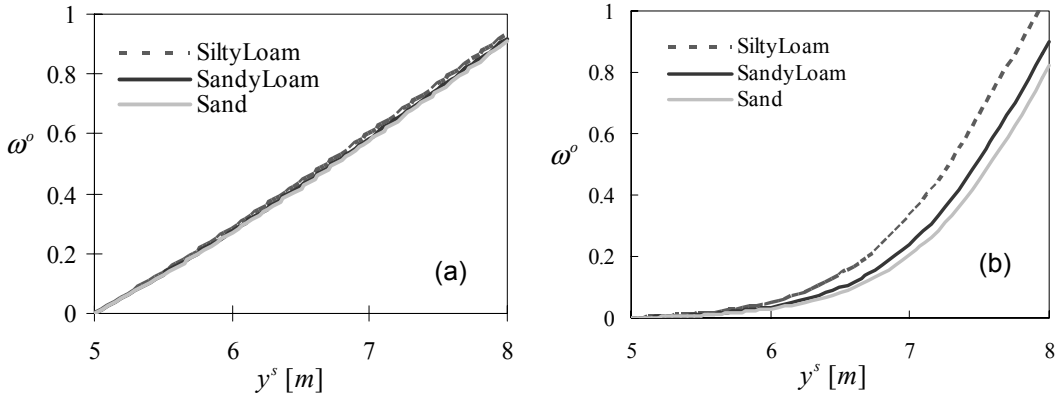

Fig. 15.3 *Saturated area fraction as a function of saturated zone depth for (a) linear topography; and (b) nonlinear topography.*

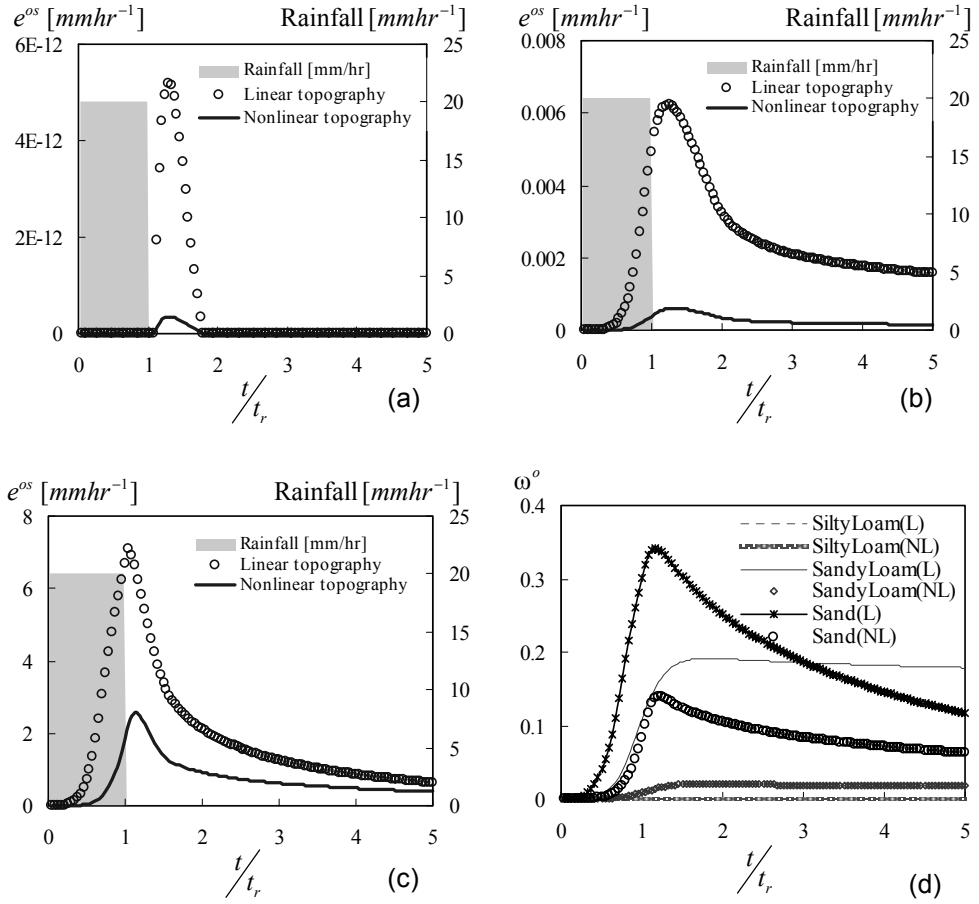

Fig. 15.4 *Sensitivity tests of closure relationship for seepage flux: (a) silty loam; (b) sandy loam; (c) sand; (d) the rate of change of fraction of saturated surface for (a) to (c), where L and NL denote linear and nonlinear topography for surface geometry, respectively (see also Fig. 15.3).*

time for the different soils can be explained by the role of the threshold inherent to the momentum balance of the unsaturated zone. The differences in the magnitude of the seepage flux among the three soil types are mainly due to the differences in recharge magnitude, caused by differences in hydraulic conductivity as the saturation in the unsaturated zone increases. Once again, the adopted closure relations produce physically-reasonable results expected under the circumstances.

3. Total catchment response estimated at the outlet

Figure 15.5 presents the breakdown of various processes occurring over the catchment in response to two consecutive and identical constant intensity events. The processes include infiltration, seepage outflow, saturated overland flow and channel flow. A rainfall intensity of 20 mm h^{-1} was adopted for both events, with identical climatic periods $t_a = t_r + t_b$, with $t_r = 1$ day and $t_b = 4$ days. As well, the linear topographic function was used for saturated area, and the soil type used was sand. Fixed parameter values are $DI = 2.0$, $M = 1$, $\alpha^{uc} = 1$, $\alpha^{u}_{wg} = 100$, $\alpha^{os}_{1} = 2000$ and $\alpha^{os}_{2} = 5.2$; the other parameter values used are presented in Table 15.1.

We see in Fig. 15.5 that the total saturated overland flow is a combined response of both seepage flow and rainfall falling on saturated areas. There was no Hortonian overland flow from the concentrated overland flow zone in this case, so it can be inferred that the decline of infiltration flux displayed is not caused from reduced soil infiltration capacity or surface ponding, but rather caused by the increased saturated area fraction. This is confirmed by the surface runoff caused by rainfall falling on saturated areas. At the beginning of the second climatic period, saturated overland flow exhibits a sudden jump due to rainfall falling on already saturated areas, with the infiltration rate being less than that of the first climatic period due to the increased saturated area fraction. The discharge hydrograph at the catchment outlet is almost the same as saturated overland flow, and does not show any effect of channel storage. This is partly due to the size of catchment used, and the nature of closure relations used for channel flow. The generalization of these closure relations to reflect dynamic effects, including diffusion and inertial effects is the subject of future work.

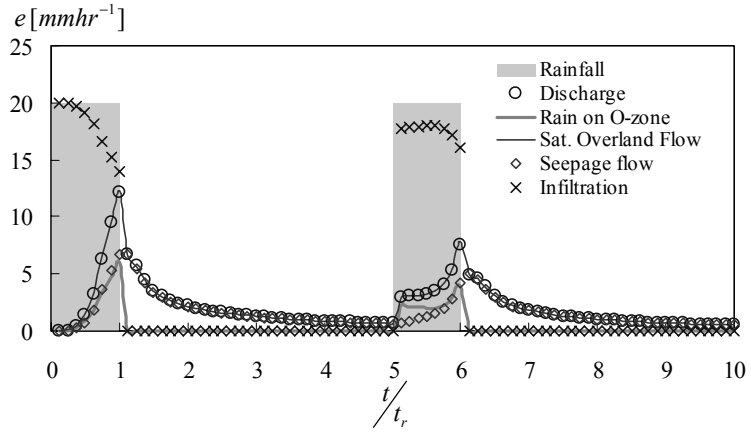

Fig. 15.5 *Saturated overland flow and total discharge at channel outlet as the integrative response of all processes occurring within the catchment.*

4. Performance of REW model as an integrative simulator of the catchment system

In order to further test the physical realism of the REW model parameterizations a numerical experiment was carried out to evaluate the predictions of the model under different combinations of climate, soil, topography and vegetation. Five different combinations were considered: two different climates, humid (DI = 0.5) and semiarid (DI = 2.0); two different soils, sandy loam and sand; two different vegetation types, fully vegetated and bare soil; two different topographies, linear and nonlinear. These five combinations are classified into five regimes summarized in Table 15.2.

Table 15.2 *Classification of numerical simulations to test the performance of the REW model as an integrative simulator of the catchment system. Note: Linearity and nonlinearity of topography is determined by three parameters:* $\beta_1^{\omega^o}$, $\beta_2^{\omega^o}$ *and* $\beta_3^{\omega^o}$; *their functional forms can be found in Fig. 15.3.*

Regime	Soil type	Dryness index	Canopy density	Topography
1	Sandy loam	2.0	1	Linear
2	Sandy loam	0.5	1	Linear
3	Sandy loam	2.0	0	Linear
4	Sandy loam	2.0	1	Nonlinear
5	Sand	2.0	1	Linear

In all cases, the experiment involved applying a rainfall of constant intensity of 10 mm h^{-1} over a period (storm duration) of 1 day, followed by an inter-storm period of 4 days. The parameter values used are $\alpha^{uc} = 1$, $\alpha_{wg}^{u} = 100$, $\alpha_1^{os} = 2000$, $\alpha_2^{os} = 5.2$ and $z^r = 25$ m, with the remainder as given in Table 15.1. The results are presented in Fig. 15.6, which not only presents (i) the rainfall and runoff response at the outlet (top panel); but also (ii) unsaturated zone soil saturation and vertical velocity (panel 2 from the top); seepage flow and saturated area fraction (panel 3); infiltration capacity at the surface and exfiltration capacity (panel 4); and, actual infiltration rate and actual exfiltration rate (bare soil evaporation and transpiration by root uptake) (panel 5).

In this way, Fig. 15.6 provides considerable insights into the internal mechanisms that contribute to the observed runoff response at the catchment outlet. In particular, we can see that the rising limb and the first peak of the runoff hydrograph closely follow the saturated area fraction, since they are generated by rainfall falling on the advancing saturated area. On the other hand, the second peak of the runoff hydrograph is linked to seepage outflow. In sandy loams, the second peak of the runoff hydrograph is hardly detectable as the seepage outflow is much smaller than rainfall falling on the saturated area, which is a result of considerably slower water movement in the subsurface zone. Recharge and capillary rise alternated between storm duration and inter-storm period, respectively, and closely follow the dynamics of the unsaturated zone soil moisture. The infiltration capacity of soil decreases during the storm period and increases during the inter-storm period, while the exfiltration capacity shows opposite behaviour. The continuous evapotranspiration process reduces saturation degree in the unsaturated zone, which subsequently induces extraction of water from the saturated zone into the unsaturated zone through capillary rise. The dynamics of seepage outflow generally follows that of the saturated area fraction, although there appears to be some hysteresis in the relationship between the two; during the wetting phase seepage flux advances more rapidly than saturated area, and declines more rapidly during the draining phase.

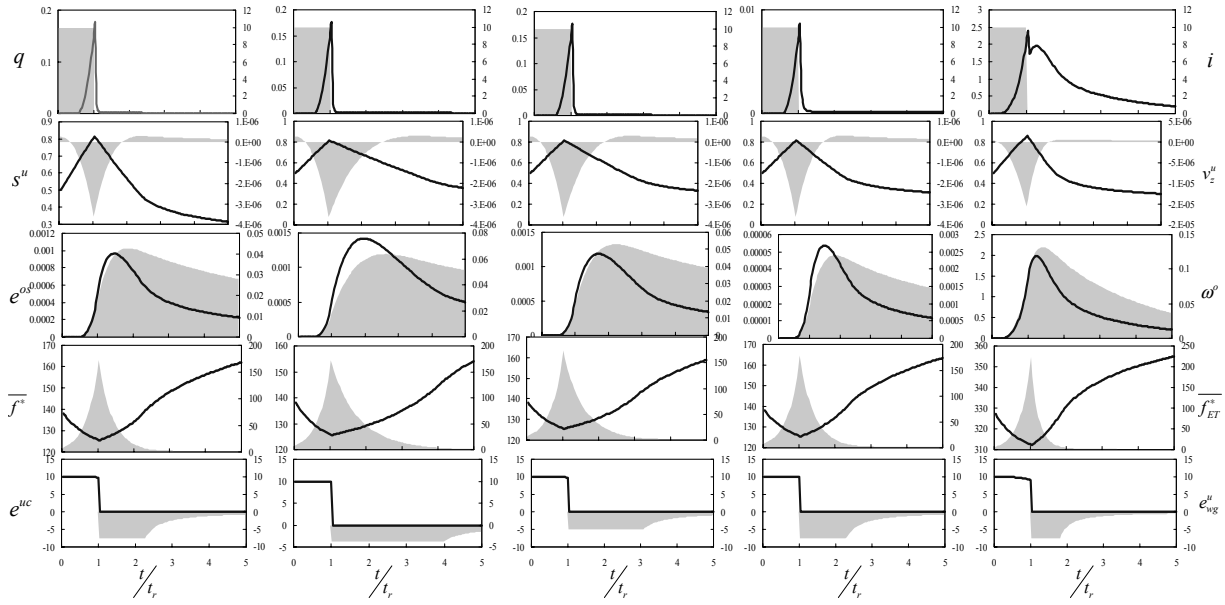

Fig. 15.6 *Sensitivity analyses of modelled whole-catchment response with respect to climate, soil, vegetation and topography. The characteristics of the different regimes are presented in Table 15.2. The left hand vertical axis of each graph refers to the solid curve, the right vertical axis refers to the shaded area. The meaning of the symbols and their units are as follows. Top panel: q (mm h^{-1}) is discharge at outlet, and i (mm h^{-1}) is rainfall intensity; panel 2 (from top): s^u is saturation degree of the unsaturated zone, and v_z^u (m s^{-1}) is vertical velocity in the unsaturated zone; panel 3: e^{os} (mm h^{-1}) is seepage outflow, and ω^o is saturated area fraction; panel 4: $\bar{f}^*$ (mm h^{-1}) is infiltration capacity, and $\bar{f}_{ET}^*$ (mm h^{-1}) is exfiltration capacity; panel 5: e^{uc} (mm h^{-1}) is actual infiltration flux, and e_{wg}^u (mm h^{-1}) is actual rate of combined bare soil evaporation and transpiration by root uptake.*

These preliminary results, and more detailed results presented in Lee *et al*. (2005b), confirm that the REW-scale model is performing in an expected and adequate manner.

We can now compare the performance of the model under different hydrological regimes. Regimes 1 and 2 refer to semiarid and humid climates, respectively, but are otherwise identical. Compared to Regime 2, Regime 1 exhibits higher evapotranspiration just after rainfall ceases. The only difference between Regimes 1 and 3 is that Regime 1 is fully vegetated, and evapotranspiration is larger and this reduces the recharge to the saturated zone and contributes to a decrease of the seepage outflow. Compared to Regime 1, Regime 4 uses nonlinear topography, and this tends to reduce saturation area and also substantially reduces seepage outflow. Regime 5 uses sand, as opposed to sandy loam for Regime 1, producing larger amounts of seepage outflow, saturation area and surface runoff. This is mainly caused by the smaller suction pressure and larger hydraulic conductivity in sandy soils for a given saturation, which induce larger recharge and the follow-on effects on seepage outflow and saturation area dynamics.

Preliminary application to Susannah Brook Catchment, Western Australia

Susannah Brook catchment (Fig. 15.7) in the southwest of Western Australia was selected as the study area for our preliminary model application. The catchment area of Susannah Brook is 23 km^2, and mean annual values of rainfall, pan evaporation and streamflow are 975 mm, 2050 mm, and 5×10^6 m^3 $year^{-1}$, respectively (Turner & Macpherson, 1990). The rainfall and pan evaporation exhibit strong seasonality but are perfectly out of phase, with the prevailing climate consisting of cold, wet winters and warm, dry summers. Hourly measurements of streamflow, potential evaporation and rainfall are available for this catchment.

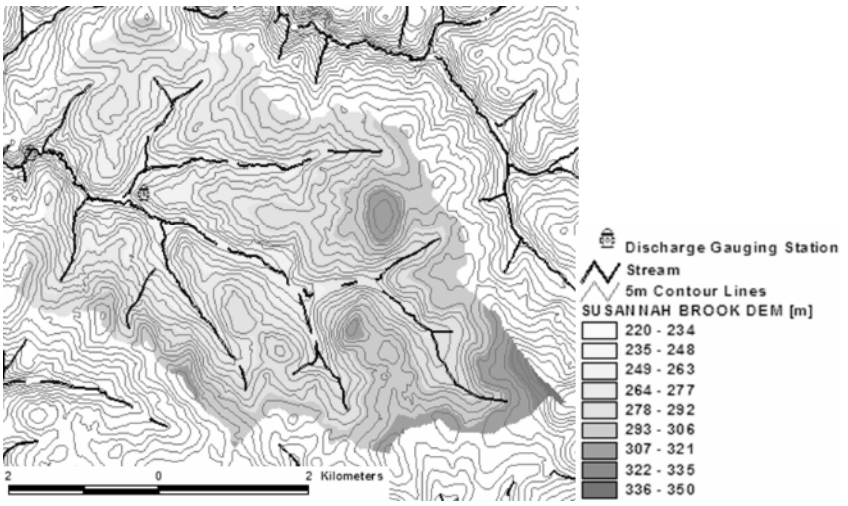

Fig. 15.7 *Map of the Susannah Brook catchment, with 5-m surface contours, streamline, surface elevation, and the locations of discharge gauging stations.*

The catchment was divided into nine REWs for this application, which were delineated with the aid of a geographic information system (GIS) by imposing a threshold area of 2 km^2 to a 10×10 m resolution digital elevation model (DEM). Subsequently, geometric information such as channel length, channel slope, the areas of the REWs, etc., were extracted from the map. The time step used for numerical simulations was 5 minutes. For this example, hourly measurements taken during the year 1982 were used in the model calibration. Manual calibration was used for estimating model parameters instead of automatic calibration methods. Therefore, the resulting parameters are preliminary only, i.e. they are not optimal. The input information, and the resulting parameter set are as follows: $k_v = 1.0$, $\overline{K}_s = 0.0000024$ m s^{-1}, $M = 0.35$ (Turner & Macpherson, 1990), $m = 1.573$, $n^c = 0.07$ $m^{-1/3}$ s, $n^o = 0.035$ $m^{-1/3}$ s, $n^r = 0.03$ $m^{-1/3}$ s, $q_s = 0.00012$ mm h^{-1}, $Z = 8$ m, $\alpha^{oc} = 1.5$, $\alpha_1^{os} = 800.0$, $\alpha_2^{os} = 0.6$, $\alpha_3^{os} = 9.0$, $\alpha^{ro} = 2.5$, $\alpha^{uc} = 1.0$, $\alpha_{wg}^{u} = 15.0$, $\varepsilon = 0.35$, $\Psi_b = 0.964$ m. The physical meaning of each parameter, their ranges of variability to keep them realistic for the area, and more sophisticated methodologies for the estimation of parameter values, should all be carefully investigated through application of the model to different settings of initial and boundary conditions. This is left for future research.

Figure 15.8 shows initial results from a model application on Susannah Brook, where the number of REWs was limited to one, meaning the whole catchment is treated as a single REW. Figure 15.8(a) describes predicted annual water balance partitioning, (b) the monthly variation of water yield (runoff), (c) flow duration curve, and (d) the daily streamflow hydrograph for the whole year. Based on the annual water balance predictions, all the rainfall falling on the concentrated overland flow zone is infiltrated, and so the main runoff generation mechanisms contributing to streamflow are subsurface storm flow and saturated excess overland flow; this accurately reflects the situation of Susannah Brook. At the monthly scale, the model under-predicts monthly water yield during the winter period. However, it follows the general trend well, suggesting that predictions could be improved by more appropriate closure relations or improved parameter estimates. In the case of the flow duration curve, we see that both high and low flow signatures are well captured by the model. Finally, predicted and observed streamflow hydrographs correspond well, and the model accurately reproduces recession limbs of the observed daily streamflows, although the peaks are not reproduced that well.

Figure 15.9 presents a validation of the model in the succeeding year, i.e. 1983, using the same parameter combinations as obtained by calibration, with different rainfall and potential evaporation inputs. It so happened that 1983 was a wetter year than 1982, which explains the increased runoff in 1983. Yet, the model does a reasonable job matching the observed runoff time series, as well as the various signatures. However, in this case, there is significant over-estimation in early winter storms, whereas in the previous year, the model under-predicted runoff during late winter storms. The flow duration curve suggests that the deeper groundwater flow is slightly over-predicted. Considering the minimal effort dedicated to the calibration, overall, it can be said that the model has done a very creditable job. This gives us confidence that the model is close to workable, and already looks like a very good new blueprint for distributed modelling.

In summary, the model predictions of water balance dynamics of Susannah Brook seems to be reasonable at all time scales. Nevertheless, there is considerable room for improvement. In particular, calibration of the model over multiple years and subsequent validation also over multiple years are likely to be more stringent tests of the model structure and closure relations, model parameter estimation, and reliability of model predictions. This is the subject of ongoing research and results will be forthcoming very shortly.

Figure 15.10 shows the result of the model performance test for the case where the catchment is divided into nine REWs, with the same parameters as used previously. Figure 15.10(a) is a discretized configuration of Susannah Brook with nine REWs. Figure 15.10(b) is a comparison of the predicted daily streamflow hydrograph with daily measured streamflow hydrograph. Daily streamflow hydrographs estimated for nine different sub-catchment areas showed negligible differences between each other. This is not surprising considering the size of the Susannah Brook catchment, and the fact that the time step for both observations and predictions is very large compared to the residence time of water in the river network. Nevertheless, the model is indeed performing well in the presence of multiple REWs. It is therefore ready to be applied to much larger catchments in Australia and overseas, wherever time of travel is much larger compared to the residence of water within the river network.

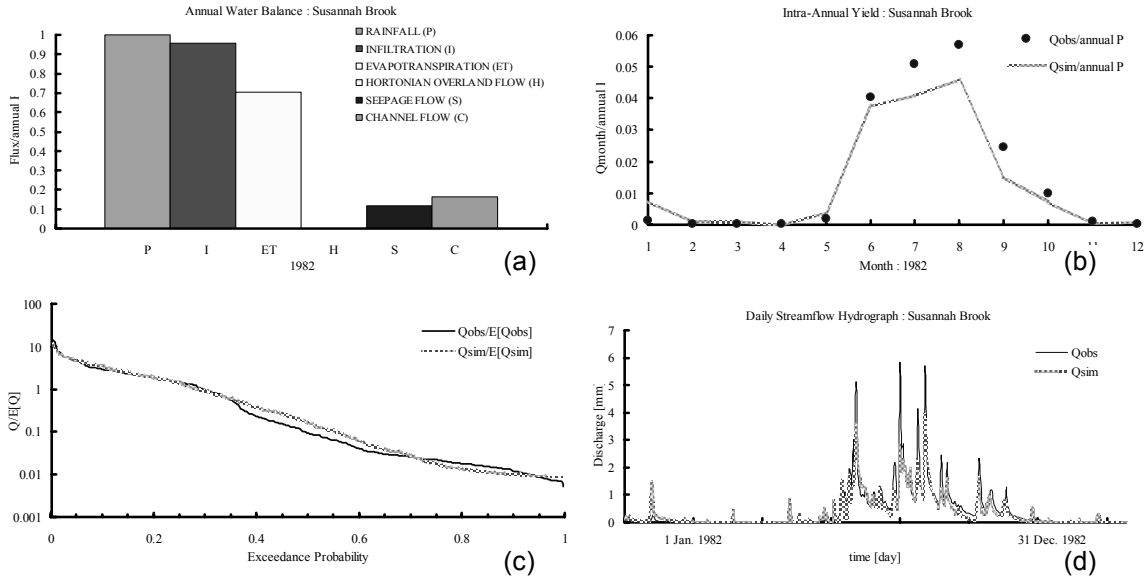

Fig. 15.8 *Signature plots at multiple time scales based on (single) REW-based model predictions obtained during the calibration phase, year 1982: (a) annual water balance partitioning; (b) intra-annual (monthly) water yield; (c) flow duration curve based on daily streamflow time series; and (d) comparison of daily streamflow hydrographs, model predicted vs observed.*

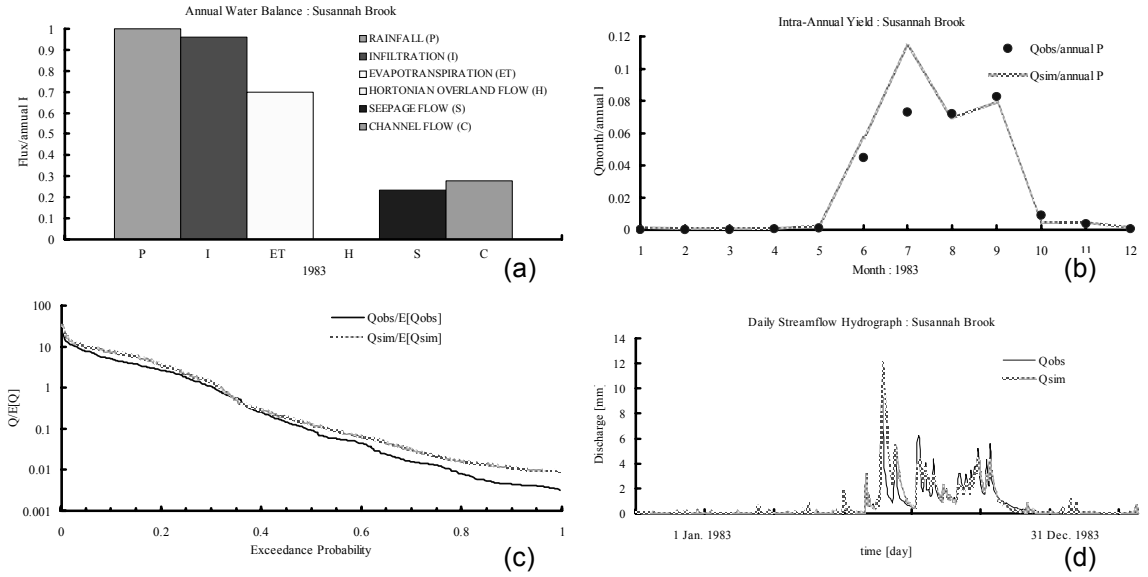

Fig 16.9 *Signature plots at multiple time scales based on (single) REW-based model predictions obtained during the validation phase, year 1983: (a) annual water balance partitioning; (b) intra-annual (monthly) water yield; (c) flow duration curve based on daily streamflow time series; and (d) comparison of daily streamflow hydrographs, model predicted vs observed.*

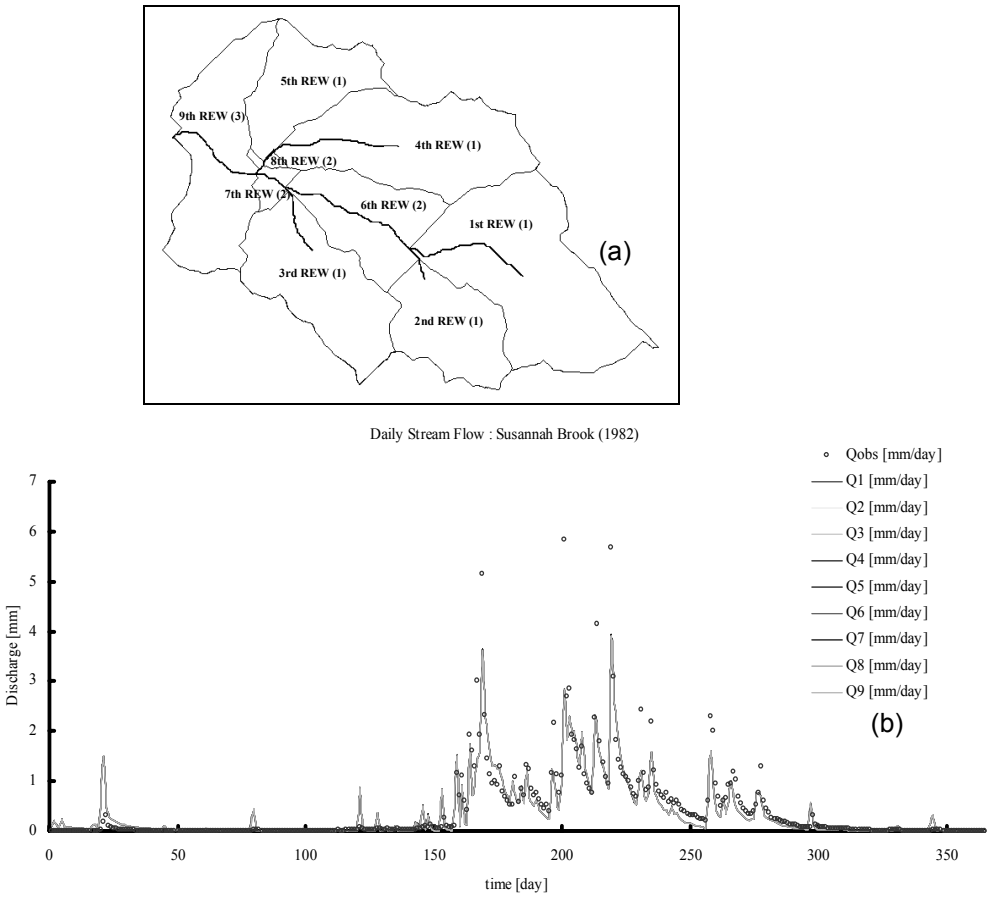

Fig. 15.10 *Predictions of a multi-REW model: (a) discretized form of Susannah Brook catchment into nine REWs, with stream order indicated in brackets; (b) daily streamflow hydrographs (model predicted vs observed).*

CONCLUSIONS

For many practical applications the advantages of truly physically-based models are clearly self-evident. This includes the ability to make predictions in ungauged basins where it is not possible to calibrate models with observed data, and the ability to predict the effects of land use or climate changes, in which case the past observations are not a sufficient guide to the future. To make hydrological models physically based, they need to satisfy two major requirements. One is consistency between the scale at which governing equations are derived and the scale at which the model is applied. This requirement is satisfied by Reggiani *et al.*'s theory since the governing equations were derived at the scale of a representative catchment, i.e. the REW scale. The second requirement is that the model should produce results consistent with observations. For this reason it is critically important that we demonstrate that the hydrological model obtained through the REW approach is physically realistic, by extracting model parameters from the catchment physical properties, and by demonstrating its relevance by applying it to real catchments. To illustrate the progress made in the REW approach

so far, we have looked at various key components of the new model blueprint. The initial application of the REW-based model, presented in this chapter, incorporated new closure relations derived for various mass and momentum exchange fluxes. Subsequent model application to the Susannah Brook catchment in Western Australia showed very promising results, and demonstrated its utility for use in distributed hydrological modelling.

There are many advantages to models based on the REW approach and the REW-scale balance equations. First of all, the models are physically-based at the scale of the REW, i.e. the scale at which prediction is usually required. Secondly, the REW approach provides balance equations defined within a unifying framework, whereas in traditional physically-based models they are derived separately. Therefore, models developed by following the REW approach should provide more internally self-consistent models. Thirdly, if adopted by different researchers and in different parts of the world, and provided the REW sub-regions remains the same, then the balance equations will remain the same, and the numerical scheme also does not need to change between applications.

All that changes are the closure relations that parameterize the various exchange fluxes. The overall framework, and the set of balance equations remain the same. Since different modellers can agree on the modelling framework, there will be improved prospects for harmonization of different models and modelling approaches. Consequently, future research in modelling can be better targeted towards both theoretical and experimental studies devoted to developing closure relations that parameterize the effects of sub-grid (i.e. sub-REW) and sub-time variabilities. Thus, the REW approach will have a direct role in the design of future field experiments, and will provide a direct vehicle for the results of field experiments to be channelled towards improved model parameterizations and predictions. Since the links between landscape properties, process understanding, and model parameterizations are explicit in this framework, the REW approach is highly amenable to estimation of predictive uncertainty, and to efforts towards reduction of predictive uncertainty through targeted efforts to reduce model structure and parameter uncertainties.

Finally, the REW approach by its design has a much sharper focus on closure relations and process conceptualizations at the REW scale, and away from the use of effective parameters to support traditional REV or point-scale physics. It is therefore much more suited to explorations of the effects of strong nonlinearities, including thresholds, on the process conceptualizations of the overall catchment behaviour. This will help us to better explain hydrological phenomena not explained in the past, and will help hydrologists with improved experimental design as well as novel modelling approaches to explicitly deal with these strong nonlinearities.

NOMENCLATURE

Latin symbols

a	coefficient of geometric relationship for average channel depth	
$\mathbf{A}$	mantle surface with horizontal normal delimiting the REW externally	
A	linearization coefficient for the mass exchange terms	$[TL^{-1}]$

b	exponent of geometric relationship for average channel depth	
B	linearization coefficient for the mass exchange terms	$[ML^{-3}]$
C	pore disconnectedness index	
$\bar{c}$	coefficient of geometric relationship for average channel width	
D	diffusivity index	
$\bar{d}$	exponent of geometric relationship for average channel width	
DI	climatic dryness index, or the ratio of annual potential evaporation to annual precipitation	
e	mass exchange per unit surface area	$[MT^{-1}L^{-2}]$
e_p	potential evaporation rate from a bare soil surface	$[LT^{-1}]$
$\bar{e}_p$	long term time average rate of potential (soil surface) evaporation	$[LT^{-1}]$
$\bar{f}^*$	spatially averaged infiltration capacity	$[LT^{-1}]$
$\bar{f}^*_{ET}$	spatially averaged exfiltration capacity on bare soil evaporation and transpiration by root uptake	$[LT^{-1}]$
g	gravitational acceleration	$[LT^{-2}]$
I	rainfall intensity	$[LT^{-1}]$
J	rate of rainfall input or evaporation	$[LT^{-1}]$
k_v	ratio of potential rates of transpiration and soil surface evaporation	
$\bar{K}$	hydraulic conductivity at the catchment scale	$[LT^{-1}]$
K_s	saturated hydraulic conductivity at the point scale	$[LT^{-1}]$
$\bar{K}_s$	saturated hydraulic conductivity at the catchment scale	$[LT^{-1}]$
l^r	the length of a channel reach	[L]
M	vegetated fraction of land surface, or canopy density	
m	pore size distribution index	
m^r	average cross sectional area	$[L^2]$
n	Manning roughness coefficient	$[TL^{-1/3}]$
p	pressure	$[FL^{-2}]$
P	the wetted perimeter	[L]
q	discharge at the outlet	$[LT^{-1}]$
q_s	steady flow from saturated zone to channel reach	$[LT^{-1}]$
R	first order friction term	$[FTL^{-3}]$
$\bar{R}$	hydraulic radius	[L]
s	saturation function of unsaturated zone	
t	time	[T]
t_a	climatic period (= $t_r + t_b$)	[T]
t_b	inter-storm period	[T]
t_r	storm period	[T]
U	second order friction term	$[FT^2L^{-4}]$
v	velocity of bulk phases	$[LT^{-1}]$
w^r	top width of the channel	[L]
y	average vertical thickness	[L]
Z	average thickness of the subsurface zone	[L]
z^r	average elevation of channel bed from datum	[L]
z^s	average elevation of the bottom end of the REW from datum	[L]

Greek symbols

α,β	parameter	
γ^j	slope angle of i-sub region flow plane with respect to horizontal plane	
Λ^{co}	contour curve separating the two overland flow zone from each other	
Λ^{or}	contour curve forming the edge of the channel	
δ_l	local angle between the reach of the REW l and the reach of the REW under consideration	
ε	soil porosity	
ϕ	the gravitational potential	
μ	the chemical potential	
ρ	water mass density	$[ML^{-3}]$
Σ	projection of the total REW surface area onto the horizontal plane	$[L^2]$
Σ^i	projection of the i-sub region surface area onto the horizontal plane	$[L^2]$
ξ^r	the length of the main channel reach per unit surface area projection	$[L^{-1}]$
Ψ	soil suction pressure head at unsaturated zone	[L]
Ψ_b	bubbling pressure head	[L]
ω	time averaged surface area fraction	

Subscripts and superscripts

u,s,c,o,r	superscripts indicating subregions within a REW
l	subscript indicating the various REWs within the watershed
w,g	designate the water and the gaseous phase respectively
$\underset{ext}{jA}$	exchange from the j-subregion across the external watershed boundary
$\underset{l}{jA}$	exchange from the j-subregion across the lth mantle segment

References

Atkinson, S. E., Sivapalan, M. & Woods, R. A. (2002) Climate and landscape controls on water balance model complexity over changing time scales. *Water Resour. Res.* **38**, 1314–1330. DOI 10.1029/2002WR001487.

Bergström, S. (1995) The HBV model. In: *Computer Models of Watershed Hydrology* (ed. by V. P. Singh), chap. 13, 443–476. Water Resources Publications, Highland Ranch, Colorado, USA.

Beven, K. J. (1989) Changing ideas in hydrology—The case of physically based models. *J. Hydrol.* **105**, 157–172.

Beven, K. J. (1993) Prophecy, reality and uncertainty in distributed hydrological modelling. *Adv. Water Resour.* **16**, 41–51.

Beven, K. J. (2002) Towards an alternative blueprint for a physically based digitally simulated hydrologic response modelling system. *Hydrol. Processes* **16**, 189–206.

Beven K. J. & Binley, A. (1992) The future of distributed models: Model calibration and uncertainty prediction. *Hydrol. Processes* **6**, 279–298.

Cox, S. M. & Matthews P. C. (2002) Exponential time differencing for stiff systems. *J. Comput. Phys.* **176**, 430–455.

Duan, Q., Sorooshian, S. & Gupta, V. (1992) Effective and efficient global optimisation for conceptual rainfall-runoff models. *Water Resour. Res.* **28**(4), 1015–1031.

Duffy, C. J. (1996) A two-state integral-balance model for soil moisture and groundwater dynamics in complex terrain. *Water Resour. Res.* **32**(8), 2421–2434.

Ewen, J. (1997) "Blueprint" for the UP modelling system for large-scale hydrology. *Hydrol. Earth System Sci.* **1**, 55–69.

Ewen, J., Sloan W. T., Kilsby C. G. & O'Connell, P. E. (1999) UP modelling system for large-scale hydrology: deriving large-scale physically based parameters for the Arkansas Red River Basin. *Hydrol. Earth System Sci*. **3**(1), 125–136.

Farmer, D. F., Sivapalan M. & Jothityangkoon, C. (2003) Climate, soil and vegetation controls upon the variability of water balance in temperate and semiarid landscapes: downward approach to water balance analysis. *Water Resour. Res.* **39**, 1035–1055.

Freer, J., McDonnell, J. J., Beven, K., Burns, D., Hooper, R., Aulenbach, B., Kendall, C. & Peters, N. (2002) Understanding the spatial and temporal dynamic contributions of subsurface storm runoff at the hillslope scale. *Water Resour. Res.* **38**(12), 5-1–5-16.

Freeze, R. A. & Harlan, R. L. (1969) Blueprint for a physically based, digitally simulated hydrologic response model. *J. Hydrol.* **9**, 237–258.

Grayson, R. B., Moore, I. D. & McMahon, T. A. (1992) Physically-based hydrologic modelling. 2. Is the concept realistic? *Water Resour. Res.* **28**, 2659–2666.

Ichikawa, Y. & Shiiba, M (2002) Lumping of kinematic wave equation considering field capacity. *Proc. Third Int. Conf. on Water Resources and Environment Research.* **1**, 56–60.

Jothityangkoon, C., Sivapalan, M. & Farmer, D. L. (2001) Process controls of water balance variability in a large semi-arid catchment: downward approach to hydrological model development. *J. Hydrol*. **254**, 174–198.

Kees, C. E., Farthing, M. W., Band, L. E. & Miller, C. T. (2002) Choices of scale and process complexity in hillslope models. *Eos Trans. AGU* **83**(47), Fall Meeting Supplement, Abstract H62B-0838.

Kees, C. E., Band, L. E. & Farthing, M. W. (2004) Effects of Dynamic Forcing on Hillslope Water Balance Models. Technical Report CRSC-TR04-12, Center for Research in Scientific Computation, Department of Mathematics, North Carolina State University, USA.

Kirchner, J. W. (2003) A double paradox in catchment hydrology and geochemistry. *HP Today, Hydrol. Process*. **17**, 871–874. DOI 10.1002/hyp.5108.

Kuczera, G. & Parent, E. (1998) Monte Carlo assessment of parameter uncertainty in conceptual catchment models: the Metropolis algorithm. *J. Hydrol.* **211**, 69–85.

Lee, H., Sivapalan, M. & Zehe, E. (2005a) Representative Elementary Watershed (REW) approach, a new blueprint for distributed hydrologic modelling at the catchment scale: development of closure relations. In: *Predicting Ungauged Streamflow in the Mackenzie River Basin: Today's Techniques and Tomorrow's Solutions* (ed. by C. Spence, J. W. Pomeroy & A. Pietroniro), 165–218. Canadian Water Resources Association (CWRA), Ottawa, Canada.

Lee, H., Sivapalan, M. & Zehe, E. (2005b) Representative Elementary Watershed (REW) approach, a new blueprint for distributed hydrologic modelling at the catchment scale: numerical implementation. In: *Physically Based Models of River Runoff and their Application to Ungauged Basins* (ed. by P. E. O'Connell & L. Kuchment) (Proc. NATO Advanced Workshop, Newcastle-upon-Tyne, UK (in press).

Reggiani, P. & Schellekens J. (2003) Modelling of hydrological responses: the representative elementary watershed approach as an alternative blueprint for watershed modelling. *Hydrol. Processes* **17**, 3785–3789.

Reggiani, P., Sivapalan, M. & Hassanizadeh, S. M. (1998) A unifying framework for watershed thermodynamics: balance equations for mass, momentum, energy and entropy and the second law of thermodynamics. *Adv. Water Resour.* **22**(4), 367–398.

Reggiani, P., Hassanizadeh, S. M., Sivapalan, M. & Gray, W. G. (1999) A unifying framework for watershed thermodynamics: constitutive relationships. *Adv. Water Resour.* **23**(1), 15–39.

Reggiani, P., Sivapalan, M. & Hassanizadeh, S. M. (2000) Conservation equations governing hillslope responses: exploring the physical basis of water balance. *Water Resour. Res.* **36**, 1845–1863.

Reggiani, P., Sivapalan, M., Hassanizadeh, S. M. & Gray, W. G. (2001) Coupled equations for mass and momentum balance in a stream network: theoretical derivation and computational experiments. *Proc. Roy. Soc. Lond.* **457**, 157–189.

Rosenbrock, H. H. (1963) Some general implicit processes for the numerical solution of differential equations. *Comput. J.* **5**, 329–330.

Sivapalan, M., Ruprecht, J. K. & Viney, N. R. (1996) Water and salt balance modelling to predict the effects of land use changes in forested catchments. 1. Small catchment water balance model. *Hydrol. Processes* **10**, 393–411.

Sivapalan, M., Takeuchi, K., Franks, S. W., Gupta, V. K., Karambiri, H., Lakshmi, V., Liang, X., McDonnell, J. J., Mendiondo, E. M., O'Connell, P. E., Oki, T., Pomeroy, J. W., Schertzer, D., Uhlenbrook, S. & Zehe, E. (2003a) IAHS Decade on Predictions in Ungauged Basins (PUB), 2003–2012: Shaping an exciting future for the hydrological sciences. *Hydrol. Sci. J.* **48**(6), 857–880.

Sivapalan, M., Blöschl, G., Zhang, L. & Vertessy, R. (2003b) Downward approach to hydrological prediction. *Hydrol. Processes* **17**, 2101–2111. DOI 10.1002/hyp.1425.

Sorooshian, S. & Gupta, V. K. (1995) Model Calibration, Chap. 2 in: *Computer Models of Watershed Hydrology* (ed. by V. P. Singh), 23–68. Water Resources Publications, Highland Ranch, Colorado, USA.

Thiemann, M., Trosset, M., Gupta, H. V. & Sorooshian, S. (2001) Bayesian recursive parameter estimation for hydrologic models. *Water Resour. Res.* **37**(10), 2521–2535.

Thomas, R. M. & Gladwell, I. (1985) Variable-order variable-step algorithms for second order systems, *Numerical Analysis Report 109*. Dept of Mathematics, University of Manchester, UK.

Troch, P. A., De Troch, F. P. & Brutsaert, W. (1993) Effective water table depth to describe initial conditions prior to storm rainfall in humid regions. *Water Resour. Res.* **29**(2), 427–434.

Turner, J. V. & Macpherson, D. K. (1990) Mechanisms affecting streamflow and stream water quality: An approach via stable isotope, hydrogeochemical, and time series analysis. *Water Resour. Res.* **26**(12), 3005–3019.

Zehe, E., Lee, H. & Sivapalan, M. (2005) Derivation of closure relations and commensurate state variables for mesoscale hydrological models using dynamical upscaling. In: *Predictions in Ungauged Basins*: *International Perspectives on the State of the Art and Pathways Forward* (ed. by S. W. Franks, M. Sivapalan, K. Takeuchi & Y. Tachikawa), 134–158. IAHS Publ. 301. IAHS Press, Wallingford, UK (this volume).